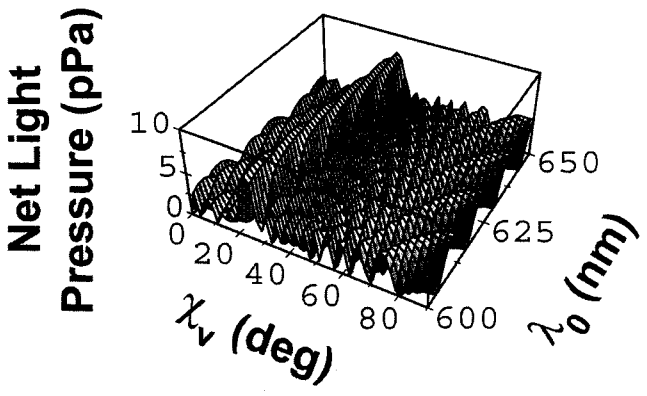

Figure 4 Net light pressure as a function of χ_v and λ_0, calculated for the same conditions as for Figure 3 with the frequency-dispersion of $\varepsilon_{a,b,c}$ ignored over the λ_0-range. [Color figure can be viewed in the online issue, which is available at www.interscience.wiley.com]

expressions are applicable to CTFs produced by one particular experimental apparatus, but may have to be modified for CTFs produced by others on different apparatuses; hence, we used these expressions for the numerical results presented in this communication merely for illustration.

3. NUMERICAL RESULTS AND DISCUSSION

Four reflectances (R_{RR}, R_{LR}, R_{RL}, and R_{LL}) and four transmittances (T_{RR}, T_{LR}, T_{RL}, and T_{LL}) can be formulated for a chiral STF [1], where the subscript RL indicates Right-circularly polarized reflected/transmitted light when the incident light is Left-circularly polarized, and so on. The net light pressure on the chiral STF is formulated via the Maxwell stress dyadic, as shown elsewhere [6].

For the numerical results presented in this section, the thickness of the chiral STF was fixed at 6 μm, and the film was taken to be structurally right-handed. Equations (3)–(6) were used for $\varepsilon_{a,b,c}$ and χ as functions of the vapor incidence angle. We set $\Omega = 166$ nm so that the Bragg center-wavelength [1]

$$\lambda_0^{Br} = \Omega\left[\left(\frac{\varepsilon_a\varepsilon_b}{\varepsilon_a\cos^2\chi + \varepsilon_b\sin^2\chi}\right)^{1/2} + \varepsilon_c^{1/2}\right] \qquad (7)$$

falls at ~633 nm when $\chi_v = 30°$.

All remittances of the chosen chiral STF [1] were computed at $\lambda_0 = 633$ nm as functions of χ_v, for a normally incident, right circularly polarized plane wave. The two reflectances R_{RR} and R_{LR} as well as the two transmittances T_{RR} and T_{LR} are presented in Figure 2 as functions of χ_v. A strong dependence on χ_v clearly exists, and the co-handed reflectance R_{RR} sharply increases in a fairly narrow χ_v-regime near $\chi_v = 30°$. To contextualize this value of χ_v, let us note that the circular Bragg phenomenon vanishes when $\chi_v = 16.621°$ and the bandwidth of the Bragg regime is maximum when $\chi_v = 33.26°$ [3].

Figure 3 shows the net light pressure on the chiral STF for the same conditions. A comparison of Figures 2 and 3 shows a distinct correlation between the net light pressure and the total co-handed reflectance with respect to the vapor incidence angle, with the maximums of both emerging near $\chi_v = 30°$. This correlation makes intuitive sense as follows. When a particle hits a substrate, the impulse experienced by the substrate equals the change in the momentum of the particle. Thus, the net light pressure on the chiral STF can be thought of as proportional to change of momentum of photons impinging on the chiral STF. The maximum change in photonic momentum must occur on perfect reflection; hence, we should expect the maximum net light pressure to occur concurrently with maximum reflectance. Small changes in the wavelength λ_0 cause some variation in the net light pressure, as shown in Figure 4, but the overall results are not qualitatively affected.

Thus, by proper selection of the vapor incidence angle χ_v, a mechanical consequence of the electromagnetic interaction between light and a chiral STF can be maximized, and will occur concurrently with the maximum co-handed reflectance of the chiral STF. This result is expected to be of significance for experimental verification of light-induced stresses in chiral STFs, as well as in STF nanomechanical devices utilizing the phenomenon of light pressure.

REFERENCES

1. A. Lakhtakia and R. Messier, Sculptured thin films: Nanoengineered morphology and optics, SPIE Press, Bellingham, WA, 2005.
2. Q. Wu, I.J. Hodgkinson, and A. Lakhtakia, Circular polarization filters made of chiral sculptured thin films: Experimental and simulation results, Opt Eng 39 (2000), 1863–1868.
3. A. Lakhtakia, Pseudo-isotropic and maximum-bandwidth points for axially excited chiral sculptured thin films, Microwave Opt Technol Lett 34 (2002), 367–371.
4. F. Chiadini and A. Lakhtakia, Design of wideband circular-polarization filters made of chiral sculptured thin films, Microwave Opt Technol Lett 42 (2004), 135–138.
5. E.I. Antonoyiannakis, Electromagnetic fields and forces in nanostructures, Ph.D. Dissertation, Imperial College, London, 1998 (chapter 3).
6. B.M. Ross and A. Lakhtakia, Light pressure on chiral sculptured thin films and the circular Bragg phenomenon, Optik, in press.
7. I.J. Hodgkinson, Q.H. Wu, and J. Hazel, Empirical equations for the principal refractive indices and column angle of obliquely deposited films of tantalum oxide, titanium oxide, and zirconium oxide, Appl Opt 37 (1998), 2653–2659.

NOVEL DEFECTED GROUND STRUCTURE ELEMENT WITH TRIPLE TRANSMISSION ZEROS AND ITS APPLICATION FOR MULTISPURIOUS SUPPRESSION OF MICROSTRIP PARALLEL-COUPLED-LINE BANDPASS FILTER

Sio-Weng Ting, Kam-Weng Tam, and Rui Martins
Wireless Communication Laboratory, Faculty of Science and Technology, University of Macau, Macau, China

Received 16 October 2006

ABSTRACT: *A novel compact defected ground structure (DGS) element with triple transmission zeros is proposed. The zeros can be tuned individually by the DGS geometry and the overall etched area is kept as compact as that of the conventional structure with single zero. The traditional microstrip parallel-coupled-line bandpass filter cascading this new element, not only achieves the multispurious suppression but also its basic design formulation is retained. A prototype DGS filter was designed and tested to validate its performance.* © 2007 Wiley Periodicals, Inc. Microwave Opt Technol Lett 49: 1409–1412, 2007; Published online in Wiley InterScience (www.interscience.wiley.com). DOI 10.1002/mop.22457

Key words: *defected ground structure; multispurious suppression; transmission zero; bandpass filter*

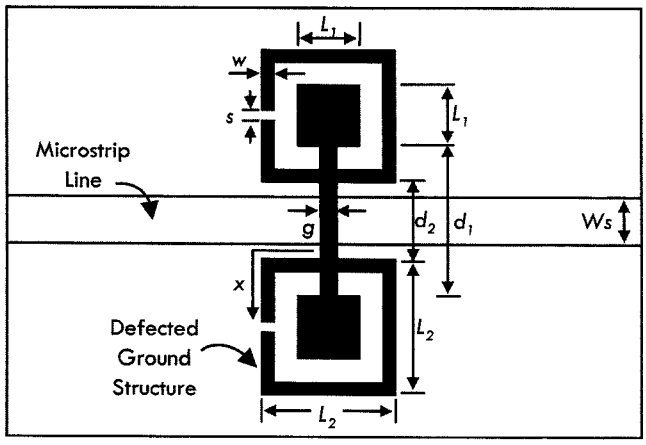

Figure 1 Proposed DGS with triple transmission zeros

1. INTRODUCTION

Traditional microstrip parallel-coupled-line bandpass filter (BPF) has been commonly used for decades, because of its simple design and implementation. However, this BPF with half-wavelength resonators suffers from spurious responses at the multiples of its center frequency f_o, i.e., nf_o (where n = 2, 3, 4, . . .). These unwanted responses indeed degrade the filter stopband performance. Recently, BPF with wide stopband has attracted larger attention, thus leading to a focus on multispurious suppression [1–3]. To suppress such spurious responses, techniques like stepped impedance resonators (SIRs) [2] or wiggly-line perturbation along the coupled-resonator edges [3] demonstrate a very wide suppression range from 2 to 6 f_o. However, both the center frequency and bandwidth are changed as the half-wavelength resonators are modified, so that the basic filter design should be reformulated or optimized.

To suppress the harmonic responses without affecting the filter basic response, a lowpass element, like defected ground structure (DGS) element, can be cascaded. The conventional DGS element has a simple microstrip line on the top and a dumbbell-shaped pattern etched in the ground plane. This DGS element exhibits a band-rejection characteristic at some frequency, which is mainly attributed by a finite transmission zero. Using this element in parallel-coupled line BPF, the first spurious harmonic can be suppressed [4]. Nonetheless, to achieve multispurious suppression, several DGS elements of different sizes are needed. This increases the circuitry size and it is also a lingering doubt of the earlier technique.

To tackle this size problem, dual rejection-band DGS elements have been reported. These DGS elements offer two transmission zeros but the defected size is kept as small as the conventional ones [5, 6]. Against this background, a novel DGS element with triple transmission zeros is proposed here. Incorporating this new element into the input or output of the conventional microstrip parallel-coupled-line BPF, three unwanted harmonic passbands can be suppressed simultaneously. In addition, the filter fundamental passband designed through conventional formulation will continue to be unaltered. This enhanced performance of the proposed BPF has been verified by simulation and measurement; and a good agreement between these results is obtained.

2. DGS WITH TRIPLE TRANSMISSION ZEROS

The proposed triple-zero DGS element is shown in Figure 1. It has a microstrip line on the top and a dumbbell-shaped pattern with slotline-enclosed lattices is etched in the ground plane. The etched dumbbell pattern has a pair of lattice with edge length of L_1 and a dumbbell-arm connected between them. The dumbbell arm has width of g and length of d_1. These two lattices are symmetrically surrounded by a slotted square loop with open ends. Each open loop with an edge length L_2 and width w intersects the dumbbell arm and the sectional length between these open loops is named d_2. The open end on each loop is determined by the open-end width of s; and also the open-end offset of x that is defined as the distance of open-end location apart from the dumbbell arm.

In this configuration, the etched pattern is symmetrically located under the microstrip line. To simplify the design process, the pair of open ends is assumed to be symmetrically placed. When one of the open-loop ends is moved in clockwise direction, the other one should be in counter-clockwise direction with the same open-end offset. To explore the frequency characteristics of the above DGS element, an example unit with L_1 = 7 mm, L_2 = 12 mm, w = g = 1 mm, d_1 = 8.53 mm, d_2 = 3.53 mm, s = 0.4 mm and x = 11 mm, and a 50-Ω microstrip line on the top has been simulated with IE3D [7] on the Rogers RO4003 substrate with a

Rui Martins: On leave from Instituto Superior Técnico, Lisbon, Portugal.

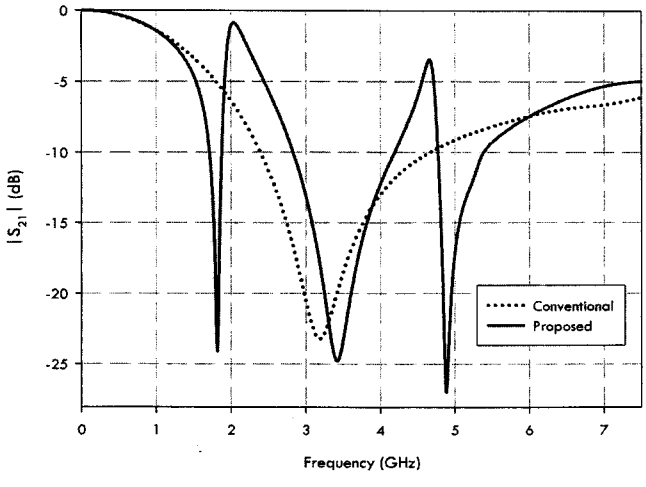

Figure 2 Simulated S_{21} of the proposed DGS and the conventional dumbbell element

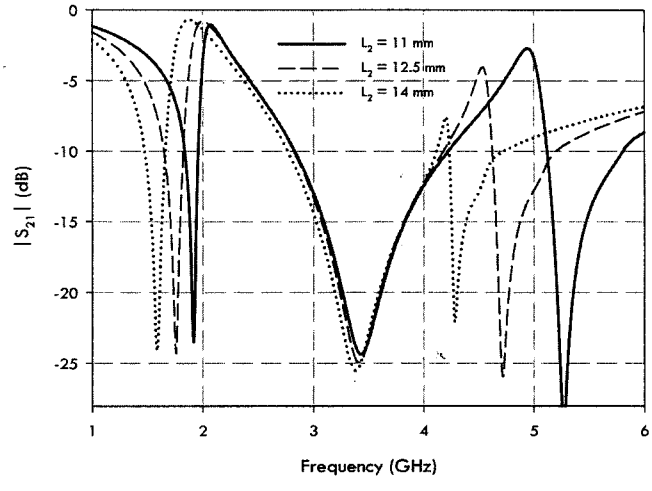

Figure 3 Simulated S_{21} of the proposed DGS element with different open-loop size L_2

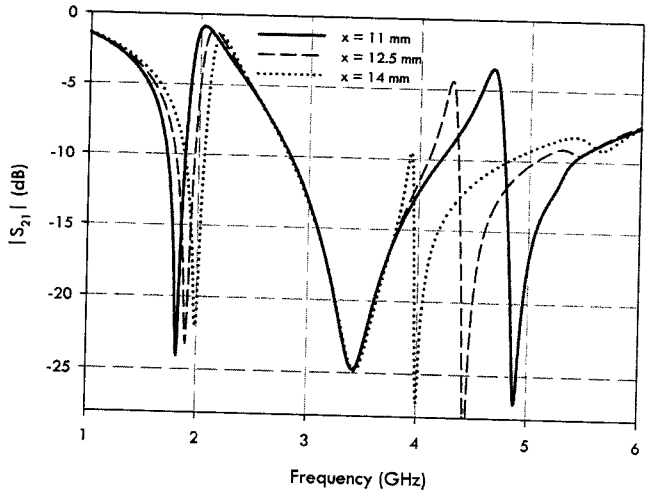

Figure 4 Simulated S_{21} of DGS element with different open-loop offset x

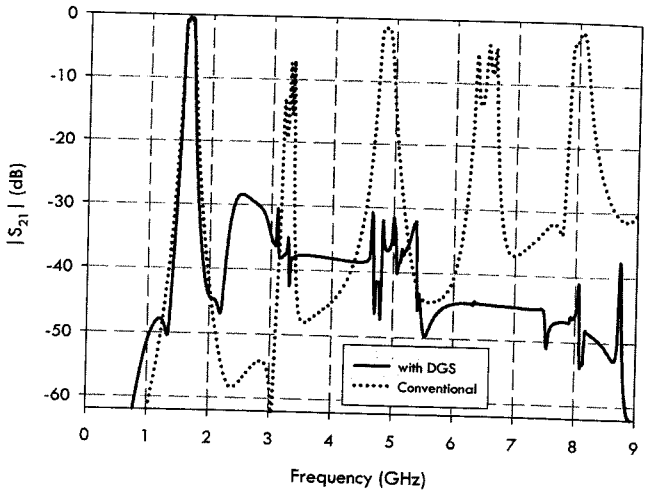

Figure 6 Simulated S_{21} of the parallel coupled-line bandpass filter

dielectric constant of 3.38 and a thickness of 1.524 mm. In contrast to the single transmission zero characteristic of the conventional dumbbell-shaped DGS unit, the frequency characteristics of the new DGS element and the conventional one with the same size are illustrated in Figure 2. It clearly shows that three finite transmission zeros at 1.81, 3.43, and 4.88 GHz are provided by this new DGS unit whilst the conventional structure only offers a transmission zero at 3.18 GHz. Moreover, the new DGS offers a much lower transmission zero frequency than the traditional dumbbell DGS; and this implies etched area reduction indeed.

To investigate the zero controllability, the earlier example of DGS element will be a simulated subject to an individual adjustment of the open-loop size (L_2), the open-end offset (x), and the inner dumbbell lattice size (L_1). In Figure 3, the transmission zero tuning property for different loop sizes is studied. Given a fixed dumbbell lattice size of $L_1 = 7$ mm, the open-loop size is adjusted from $L_2 = 11$–14 mm, it is obvious that the zeros at the lowest and highest frequencies are lowered whilst the zero at 3.43 GHz is almost unchanged. On the other hand, the effect of the open-end offset adjustment (x) is studied in Figure 4. Similarly, the zero at 3.43 GHz is retained whilst the other two zeros are further apart from each other for a smaller offset.

In addition, as shown in Figure 5, the zero near 3.43 GHz can be shifted to lower frequency when a larger lattice is used. From Figures 3 to 5, it can be confirmed that these three transmission zeros are individually controlled by the length of the longer and shorter slotline of the open loop and the lattice size of the inner dumbbell, respectively.

3. MICROSTRIP PARALLEL-COUPLED-LINE BPF WITH MULTISPURIOUS SUPPRESSION USING DGS

To verify the application of the triple-zero characteristics, the proposed DGS element is designed to suppress three harmonics of a conventional parallel-coupled-line BPF. Using the conventional design expressions, a three-order BPF with center frequency f_o = 1.6 GHz and 8% fractional bandwidth (FBW) is designed on the substrate of RO4003. On the basis of DGS properties depicted in the last section, the geometrical parameters of the DGS element are tuned to locate the three zeros at the following frequencies 2, 3, and 4 f_o, respectively. The resulted DGS element is having $L_i = 4$ mm, $L_2 = 10$ mm, $w = 1.5$ mm, $g = 3$ mm, $d_1 = 9.53$ mm, $d_2 = 3.53$ mm, $s = 0.4$ mm, $x = 14.5$ mm, and a 25-Ω microstrip line on the top. The lower impedance microstrip line is used in order to reduce the ripples in the DGS lowpass region as well as to increase the rejection bandwidth for better suppression performance.

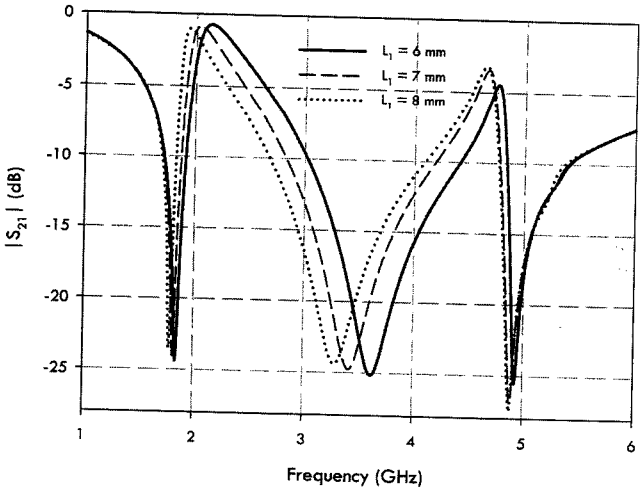

Figure 5 Simulated S_{21} of DGS element with different dumbbell lattice size L_1

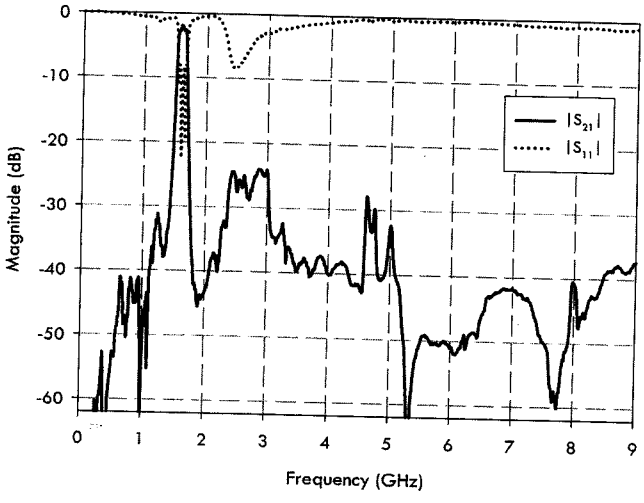

Figure 7 Measured S-parameters of the proposed DGS bandpass filter

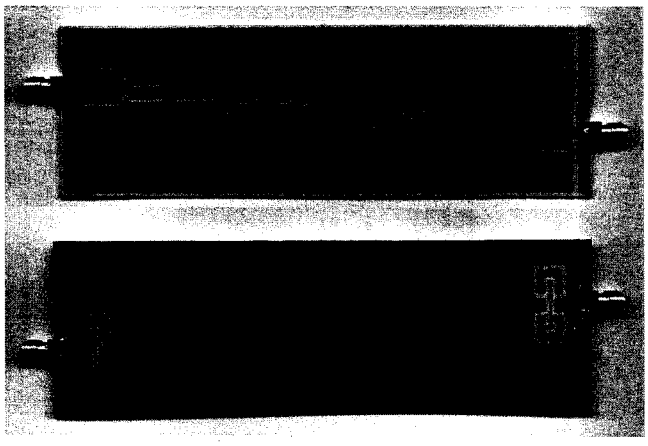

Figure 8 Photo of the prototype filter

The above parallel-coupled-line BPF embedded with the DGS element in its input and output is simulated and its frequency response is shown in Figure 6 to compare with the structure without DGS. It is obvious that not only the spurious harmonics at 2, 3, and 4 f_o are suppressed, but also the 5 f_o, which is mainly because of the wide rejection bandwidth of the zero at the highest frequency. As a result, this filter offers a wide stopband with more than 30 dB attenuation up to 5 f_o. The center frequency and bandwidth of the fundamental passband is kept as in the original filter and no significant deviation observed. The measurement results of this prototype filter have been recorded in Figure 7 and are in good agreement with the simulations. It is observed that the spurious passbands from 2 to 5 f_o are suppressed with overall 30 dB attenuation. Thus, the proposed filter outweighs the conventional structure through the multispurious suppression up to five times the center frequency. As shown in Figure 8, the size of the DGS pattern is only 10 mm × 23.5 mm and is smaller than the needed defected ground size when traditional dumbbell DGS is used to achieve similar stopband performance.

4. CONCLUSION

The proposed open-loop outlined dumbbell-shaped DGS element offers three controllable finite transmission zeros. Using this structure for multispurious suppression of BPF, unwanted passbands up to five times the center frequency can be suppressed, without significant circuitry size increase. Also, the simulated and experimental results show good agreement between them, demonstrating the usefulness of the proposed DGS unit.

ACKNOWLEDGMENT

This work has been developed under the Research Project RG066/05–06S/TKW/FST, financially supported by the Research Committee of the University of Macau.

REFERENCES

1. P. Cheong, S.W. Fok, and K.W. Tam, Miniaturized parallel coupled-line bandpass filter with spurious-response suppression, IEEE Trans Microwave Theory Tech 53 (2005), 1810–1816.
2. J.T. Kuo and E. Shih, Microstrip stepped impedance resonator bandpass filter with an extended optimal rejection bandwidth, IEEE Trans Microwave Theory Tech 51 (2003), 1554–1559.
3. T. Lopetegi, M.A.G. Laso, F. Falcone, F. Martin, J. Bonache, J. Garcia, L.P. Cuevas, M. Sorolla, and M. Guglielmi, Microstrip "Wggly-Line" bandpass filters with multispurious rejection, IEEE Microwave Wireless Comp Lett 14 (2004), 531–533.
4. J.S. Park, J.S. Yun, and D. Ahn, A design of the novel coupled-line bandpass filter using defected ground structure with wide-stopband performance, IEEE Trans Microwave Theory Tech 50 (2002), 2037–2043.
5. D.J. Woo and T.K. Lee, Suppression of harmonics in Wilkinson power divider using dual-band rejection by asymmetric DGS, IEEE Trans Microwave Theory Tech 53 (2005), 2139–2144.
6. S.W. Ting, K.W. Tam, and R.P. Martins, Miniaturized microstrip low-pass filter with wide stopband using double equilateral U-shaped defected ground structure, IEEE Microwave Wireless Comp Lett 16 (2006), 240–242.
7. IE3D User's Manual, Release 8, Zeland Software, Inc., 2001.

A 24-GHz POWER-EFFICIENT MMIC PULSE OSCILLATOR FOR UWB RADAR APPLICATIONS

Deokhwan Kim,[1] Dong-Wook Kim,[2] and Songcheol Hong[1]

[1]Department of Electrical Engineering and Computer Science, Korea Advanced Institute of Science and Technology, 373-1 Guseong-Dong, Yuseong-Gu, Daejeon 305-701, Korea

[2]Department of Radio Science and Engineering, Chungnam National University, 220 Gung-dong, Yuseong-Gu, Daejeon 305-764, Korea

Received 16 October 2006

ABSTRACT: *A 24-GHz power-efficient pulse oscillator for ultrawideband (UWB) radar applications implemented with InGaP HBT MMIC technology is proposed. The oscillator uses a common base inductive feedback topology without output buffers. The bias current is switched on by a pulse-control voltage. The oscillator consumes power only when the 24-GHz pulse is generated, allowing high power efficiency to be obtained. A high output power of 8 dBm and a low phase noise of −120 dBc/Hz at 1 MHz offset frequency are obtained in continuous wave (CW) mode. While in pulse-mode operation, the oscillator shows a 1-ns pulse width with only 5 ps of phase jitter.* © 2007 Wiley Periodicals, Inc. Microwave Opt Technol Lett 49: 1412–1415, 2007; Published online in Wiley InterScience (www.interscience.wiley.com). DOI 10.1002/mop.22456

Key words: *automotive radar; pulse oscillator; ultrawideband*

1. INTRODUCTION

Recently, extensive studies have been carried out on ultrawideband (UWB) short-range radar sensors for automotive radar applications [1, 2]. These types of radar generate short pulses by modulating a continuous wave (CW) signal using high-speed semiconductor switches, but suffer from two kinds of key problems. One is that the finite isolation of the switches causes CW-signal leakage when the switches are turned off [2]. The leakage signal radiated from an antenna is reflected from a target and interferes with the receiver's detection. The other key problem is the low power efficiency. Although no signal is emitted to the target during a switch-off period, the CW oscillator operates continuously and much energy is consumed in vain. If the radar transmitter produces a 1-ns pulse with a pulse-repetition frequency (PRF) of 30 MHz, as shown in Figure 1, only 3% of the generated energy is transmitted through the antenna.

A residual-carrier-free burst oscillator consisting of two parts, a cross-coupled LC oscillator and a current switch, was proposed to solve the CW-leakage problem [3]. This oscillator operates only when a control pulse is applied to the current switch, and does not experience CW leakages. However, the oscillator is still power-inefficient, the output buffers and current source continuously